3D assemblies of NiO nanoparticles: A precursor-modulated nanoscale-engineering from turbostratic $Ni_3(OH)_4(NO_3)_2$ and ordered β-$Ni(OH)_2$ intermediates

Biljana Pejova[1*], Arej Eid[2,3], Leonardo Lari[2,4], Ahmad Althumali[2,5], Lidija Šiller[6], Adam Kerrigan[4], Ljupcho Pejov[1] and Vlado K Lazarov[2,4*]

[1]Institute of Chemistry, Faculty of Natural Sciences and Mathematics, SS. Cyril and Methodius University, POB 162, 1000 Skopje, Macedonia

[2] School of Physics Engineering and Technology, University of York, York, UK

[3] University of Tabuk, Tabuk, Saudi Arabia,

[4] The York-JEOL Nanocentre, University of York, York, UK

[5]Department of Physics, Faculty of Science, Taif University, P.O. Box 11099, Taif 21944, Saudi Arabia

[6]School of Engineering, Newcastle University, Newcastle upon Tyne NE1 7RU, UK

e-mail: biljana@pmf.ukim.mk and vlado.lazarov@york.ac.uk

Supporting Information

- Particle size distributions and the corresponding fits.
- Additional figures from SEM and TEM measurements.
- Additional figures from temperature-dependent FTIR measurements.
- Technical details related to computation of the moving window 2D correlation spectra
- Additional figures from XPS analyses, a brief discussion concerning the assignments of the Ni $2p_{3/2}$ bands, and tabulated quantitative results from XPS measurements.
- Technical details concerning the fitting of the FTIR spectra.
- Raman spectroscopy results.
- Additional data related to the low dimensionality effects on the phonon modes studied by Raman spectroscopy.

Particle size distributions and the corresponding fits

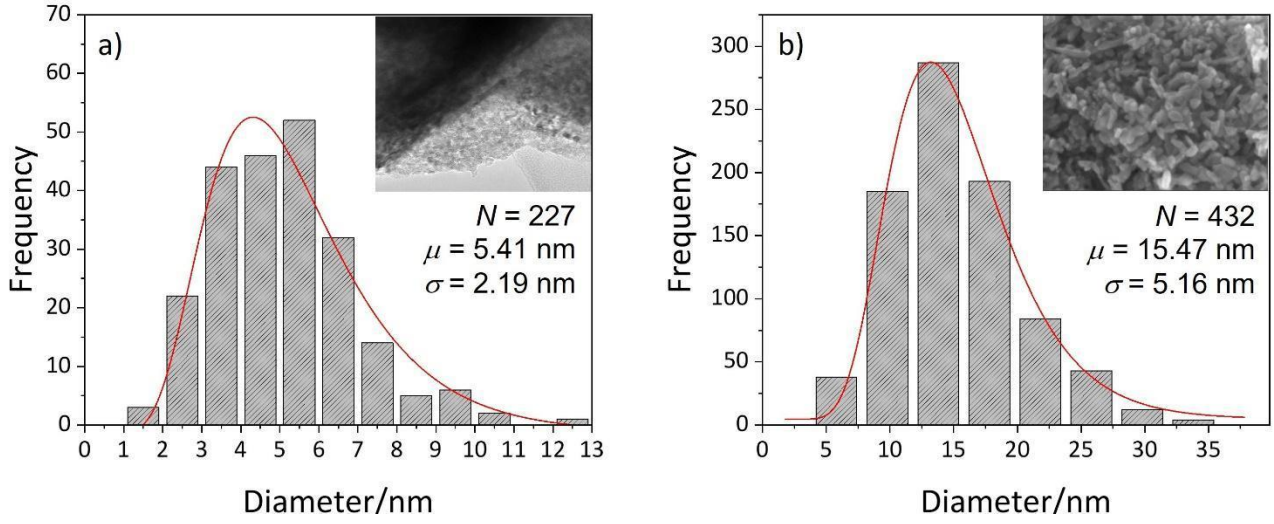

Fig. SI-1. Particle size distribution in case of NiO obtained using ammonia (a) and carbamide (b) precursors. The inset in a shows the TEM image, while the respective SEM image under the upper electron detector (UED) is shown in the inset of (b). The solid red lines are the LogNormal fitting of size distributions.

Additional figures from SEM and TEM measurements

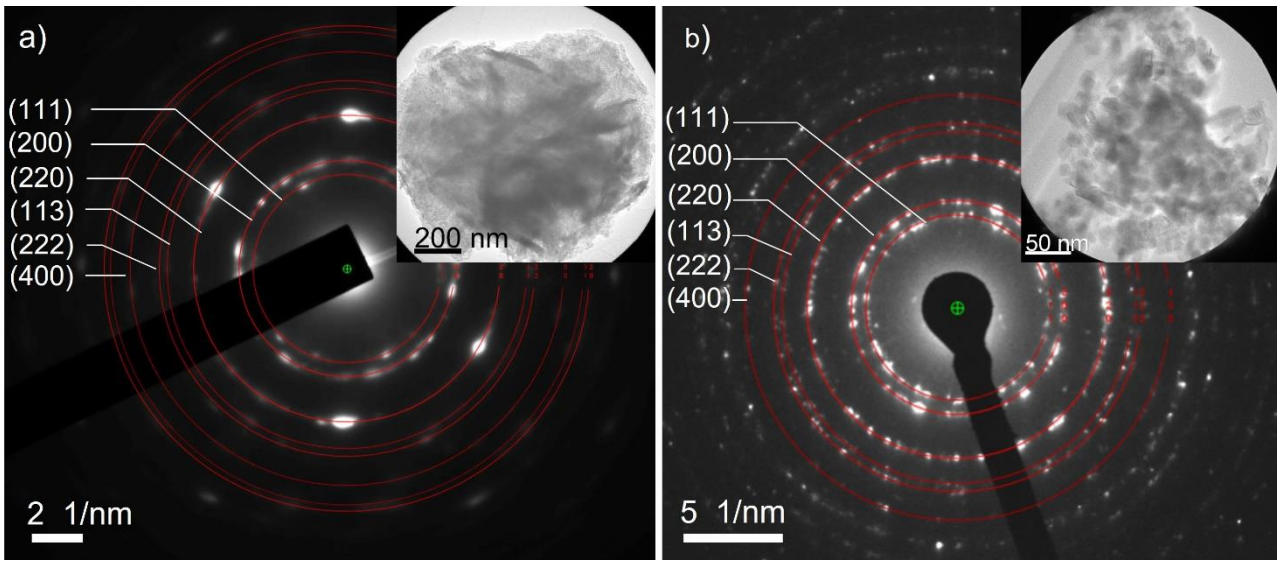

Fig. SI-2. The reference SAD patterns of cubic NiO superimposed on experimental SAD patterns of final products when ammonia (a) and carbamide (b) are used as hydroxide precursors. In agreement with the results obtained from the powder XRD measurements, the SAD patterns of final products of two developed chemical routes clearly show the rock-salt cubic structure of the NiO NPs in both cases.

Surface faceting od NiO obtained by ammonia and carbamide route

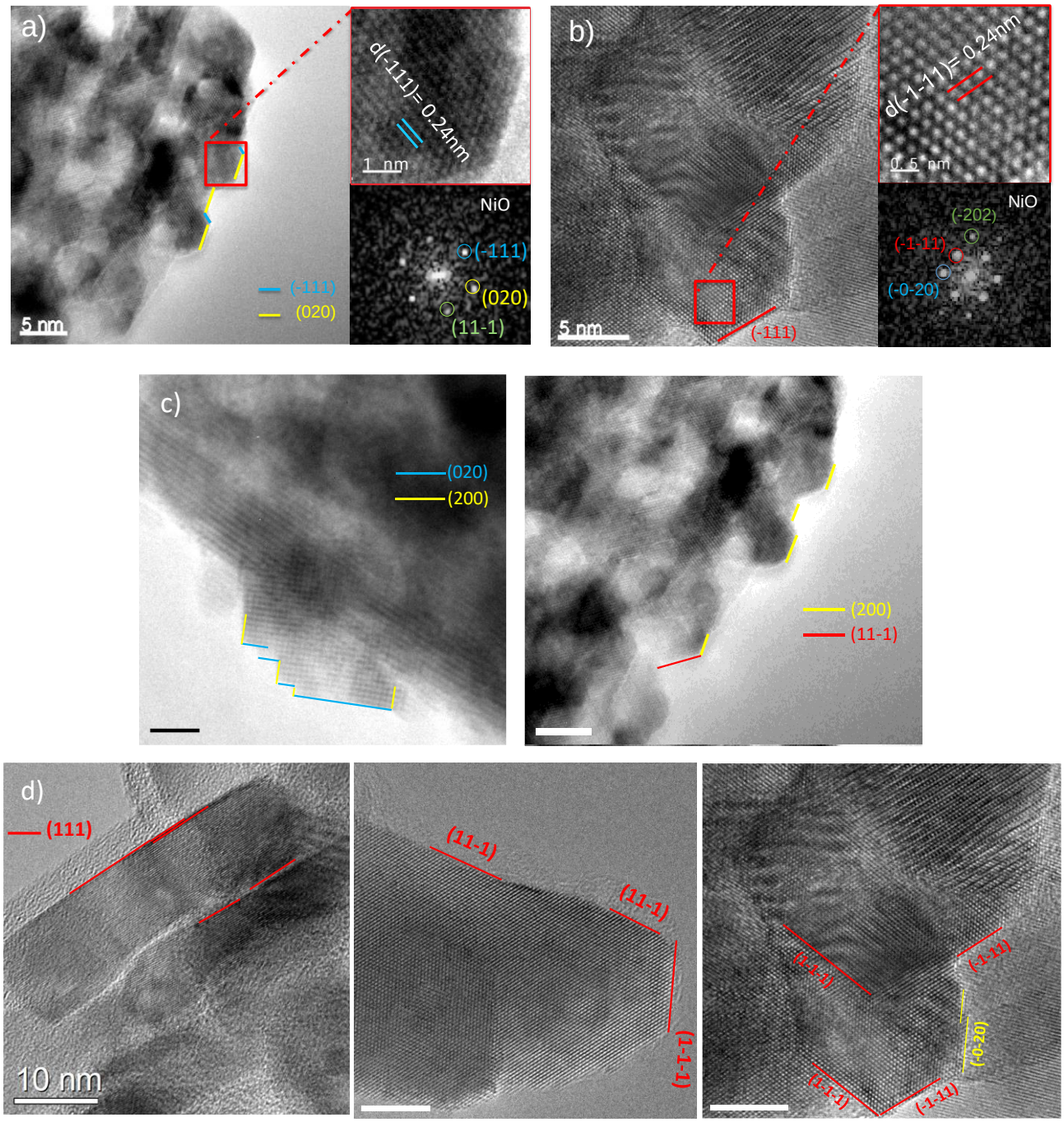

Fig. SI-3. HRTEM images of NiO obtained with thermal treatment of $Ni(OH)_2$ (a) and $Ni_3(OH)_4(NO_3)_2$ (b). Selected areas illustrate the atomic planes of the NiO along the [101] direction, as confirmed by the FFTs below selected areas. HRTEM images of different NiO NPs obtained with thermal treatment of $Ni(OH)_2$ (c) and $Ni_3(OH)_4(NO_3)_2$ (d) with the outlined type of faceting.

Additional figures from temperature-dependent FTIR measurements

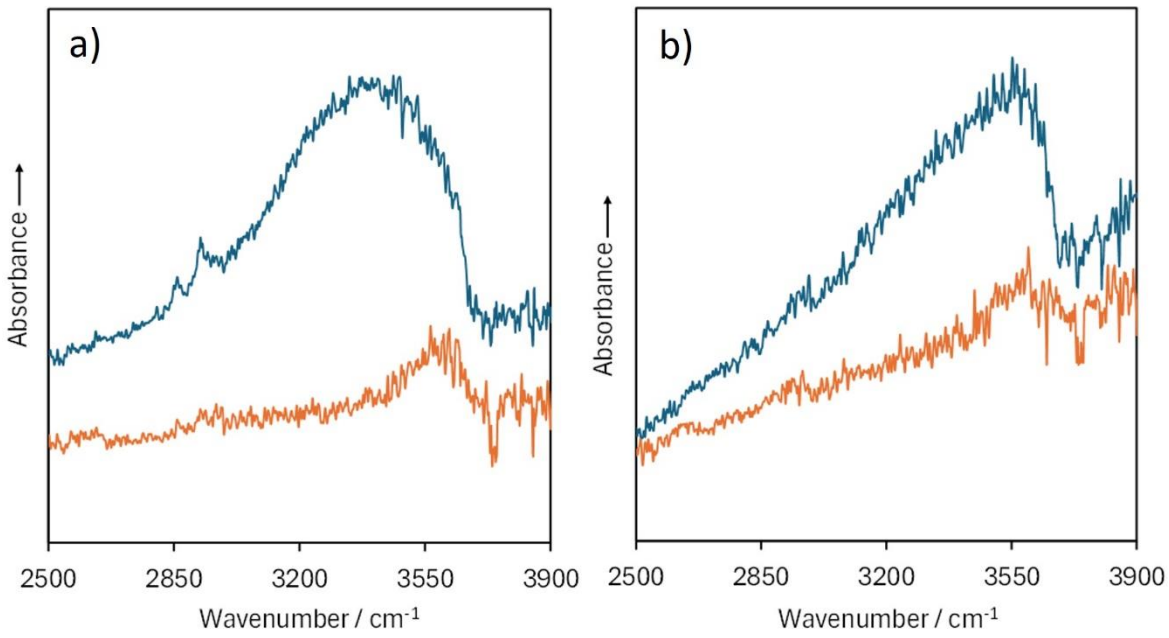

Fig. SI-4. The O-H stretching region in the temperature-dependent ATR FT-IR spectra of NiO nanoparticles synthesized by the ammonia route (a) and carbamide route (b); the temperature increases from 20 °C to 200 °C from the uppermost curve downwards.

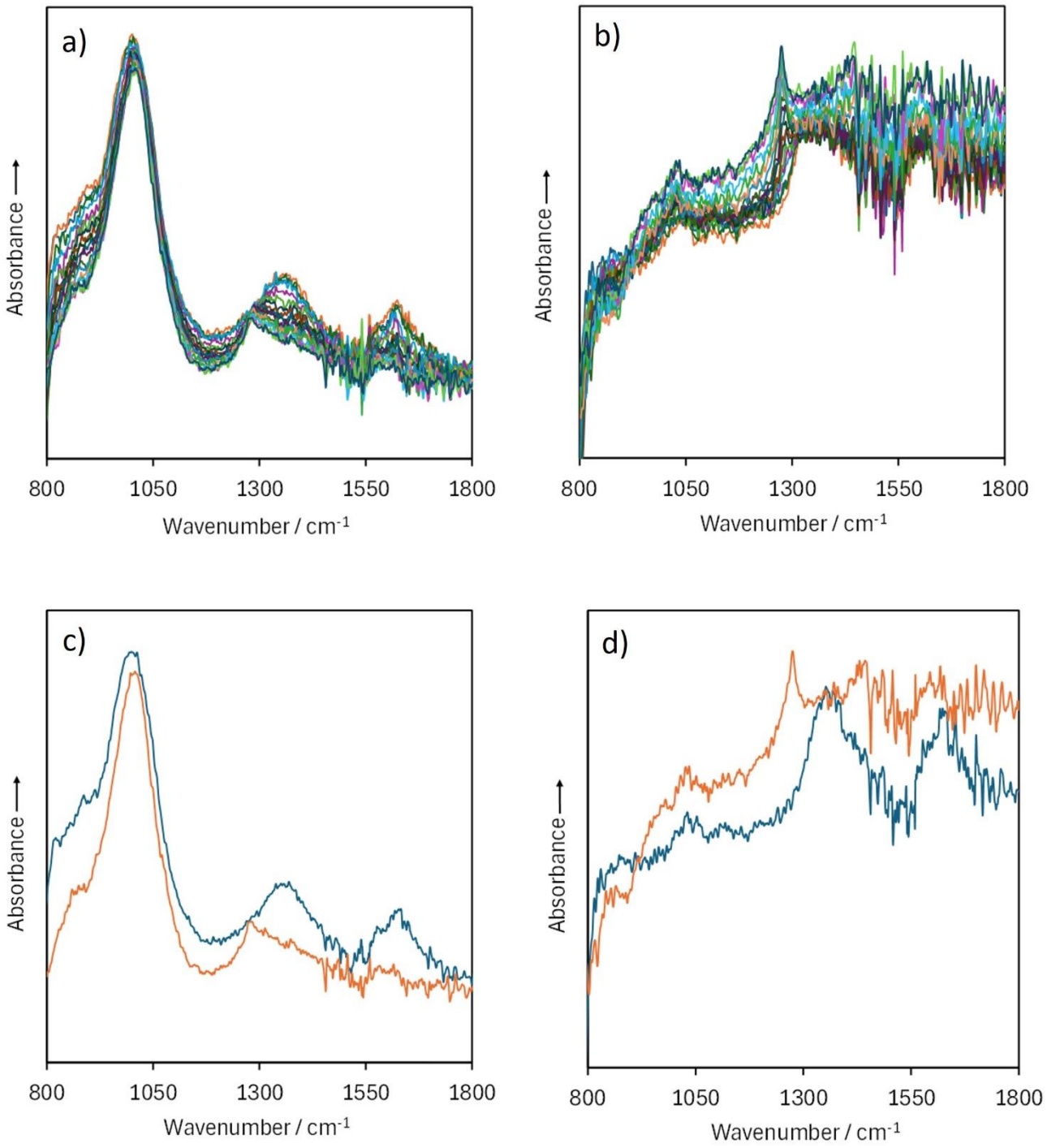

Fig. SI-5. The region of HOH bending modes in the temperature-dependent ATR FT-IR spectra of NiO NPs synthesized by the ammonia route (a and c) and carbamide route (b and d); the temperature increases from 20 °C to 200 °C from the uppermost curve downwards.

Technical details related to computation od the moving window 2D correlation spectra

The moving-window two-dimensional correlation spectra (MW 2DCOS), computed on the basis of temperature-dependent FTIR data in the present study, are based on the generalized two-dimensional correlation analysis [SI-REF-1, SI-REF-2].

In our present study, we use the change in temperature as an external perturbation to our physical system (NiO-a and NiO-c NPs). We define the "dynamic" spectrum with the expression [SI-REF-1, SI-REF-2]:

$$\tilde{y}(\tilde{\nu},T)=\begin{cases} y(\tilde{\nu},T)-\tilde{y}(\tilde{\nu}) & \text{for} \quad T_1\le T\le T_2 \\ 0 & \text{otherwise} \end{cases} \qquad \text{(SI-1)}$$

In eq. (SI-1), (T_1, T_2) is the interval within which the external perturbation is applied (*i.e.* the investigated temperature interval in our case), and $\tilde{y}(\tilde{\nu})$ is the so-called reference spectrum. For the purpose of the present study, we have defined the reference spectrum as the temperature-averaged spectrum, *i.e.*:

$$\tilde{y}(\tilde{\nu}_j)=\frac{1}{m}\sum_{i=1}^{m} y(\tilde{\nu}_j,T_i) \qquad \text{(SI-2)}$$

The generalized 2DCOS is defined with:

$$\Phi(\tilde{\nu}_1,\tilde{\nu}_2)+i\Psi(\tilde{\nu}_1,\tilde{\nu}_2)=\frac{1}{\pi(T_2-T_1)}\int \tilde{Y}_1(\omega)\cdot Y_2^*(\omega)\mathrm{d}\omega \qquad \text{(SI-3)}$$

In (SI-3), $\tilde{Y}_1(\omega)$ and $Y_2^*(\omega)$ are Fourier transform (and the corresponding conjugate pair) from the perturbation to the Fourier frequency domains of the spectral variations at the spectroscopic variable $\tilde{\nu}_1$ and $\tilde{\nu}_2$ respectively. The so-called synchronous and asynchronous 2D correlation spectra are defined with:

$$\Phi(\tilde{\nu}_1,\tilde{\nu}_2)=\frac{1}{m-1}\sum_{i=1}^{m}\tilde{y}(\tilde{\nu}_1,T_i)\cdot\tilde{y}(\tilde{\nu}_2,T_i) \qquad \text{(SI-4)}$$

and

$$\Psi(\tilde{\nu}_1,\tilde{\nu}_2)=\frac{1}{m-1}\sum_{i=1}^{m}\tilde{y}(\tilde{\nu}_1,T_i)\cdot\sum_{k=1}^{m}N_{ik}\tilde{y}(\tilde{\nu}_2,T_k) \qquad \text{(SI-5)}$$

In the last equation (SI-5) N_{ik} denotes the Hilbert-Noda transformation matrix element:

$$N_{ik} = \begin{cases} 0 & \text{if } i = k \\ \frac{1}{\pi(k-i)} & \text{otherwise} \end{cases} \quad \text{(SI-6)}$$

Considering the case when $\tilde{\nu}_1 = \tilde{\nu}_2$ in (SI-4), we arrive at the so-called autocorrelation spectrum (also called variance spectrum):

$$\Phi(\tilde{\nu}) = \frac{1}{m-1}\sum_{i=1}^{m} \tilde{y}^2(\tilde{\nu}, T_i) \quad \text{(SI-7)}$$

If we consider a data set consisting of 2*n* + 1 spectra around the *j*-th spectrum, represented in a matrix form as:

$$y_j(\tilde{\nu}, T_J) = \begin{bmatrix} y(\tilde{\nu}, T_{j-n}) \\ y(\tilde{\nu}, T_{j-n+1}) \\ \vdots \\ y(\tilde{\nu}, T_{j-n}) \\ \vdots \\ y(\tilde{\nu}, T_{j+n}) \end{bmatrix} \quad \text{(SI-8)}$$

The autocorrelation spectrum which we construct from the 2*n* + 1 spectra in the "data window" has been calculated as:

$$\Omega_{\mathrm{A},j}(\tilde{\nu}, T_j) = \frac{1}{2n}\sum_{J=j-n}^{j+n} \tilde{y}_j^2(\tilde{\nu}, T_J) \quad \text{(SI-9)}$$

Finally, the MW 2DCOS spectrum has been computed by an incremental "sliding" of the "window" throughout the complete dataset, *i.e.* from *j* = 1 + *n* to *j* = *N* – *n* [SI-REF-3]. It has been reported [SI-REF-4] that the intensity in the MW 2D correlation spectra is proportional to the square of the derivative with respect to the perturbation variable, *i.e.*:

$$\Omega_{\mathrm{A}}(\tilde{\nu}, T) \sim \left[\frac{\partial y(\tilde{\nu},T)}{\partial T}\right]_v^2 \quad \text{(SI-10)}$$

Additional figures from XPS analyses, a brief discussion concerning the assignments of the Ni $2p_{3/2}$ bands, and tabulated quantitative results from XPS measurements

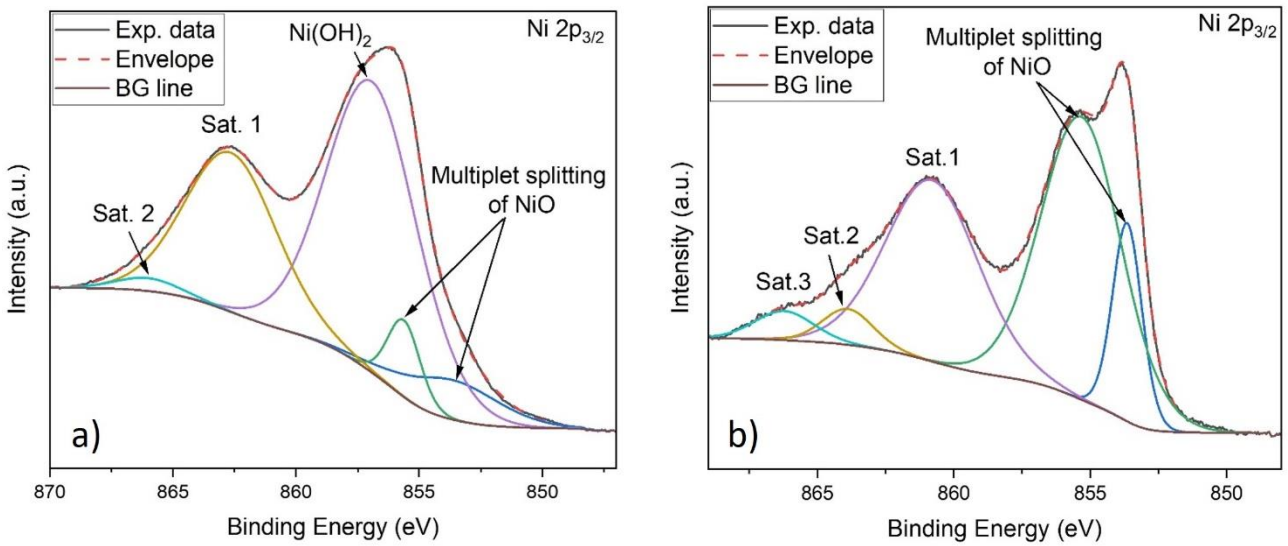

Fig. SI-6. XPS spectra of NiO NPs synthesized by the ammonia (a) and carbamide (b) routes in the regions of Ni 2p3/2 multiplet bands.

We assign the two Ni $2p_{3/2}$ bands in the studied samples to the photoemission which is accompanied by a certain valence band electron rearrangements, *i.e.*:

$2p^6\,3d^8 + h\nu \rightarrow 2p^5\,3d^8 + e^-$

and

$2p^6\,3d^8 + h\nu \rightarrow 2p^5\,3d^9\underline{L} + e^-$

where in the second equation $\underline{L}$ stands for the "ligand", *i.e.* a hole in the oxygen (O) 2*p* level ("screening" by the O 2*p* valence band). The first of the two most prominent Ni $2p_{3/2}$ bands appearing at lower binding energy (BE) values are thus assigned to photoemission of the screened core hole (the second of the above equations), the screening being from local lattice oxygen, adjacent to the Ni 2*p* core hole. The second one can, on the other hand, be assigned to the nonlocally screened core hole photoemission, with possible surface states' contribution. Table Z contains the quantitative XPS data obtained by the fitting procedure.

Table SI-1. Quantitative XPS data obtained by fitting the experimental bands (all BE-s in eV, the values in parentheses refer to the relative intensities [SI-Ref-5 – SI-Ref-11])

Specimen	Ni – bands					
	Ni $2p_{3/2}$			Satellite bands		
NiO – a	853.55 (1.00)	856.63 (0.81)	856.92 (8.21)	862.66 (4.51)	866.03 (0.25)	
NiO – c	853.65 (1.00)	855.32 (3.93)		860.80 (2.90)	863.89 (0.31)	866.22 (0.29)
	O – bands					
	O 1*s*					
NiO – a	527.17 (1.00)	529.05 (1.31)	530.61 (2.42)	531.76 (5.91)		
NiO – c	528.25 (1.00)	529.25 (12.7)	531.00 (7.49)			

Technical details concerning the fitting of FTIR spectra

The band due to the fundamental vibrational transition of the lattice OH group in the FTIR spectrum of the β-$Ni(OH)_2$ intermediate could be excellently modeled by fitting with three component bands (Fig. 10a), each a linear combination of a Gaussian and Lorentzian function (see the Supporting information for the details concerning the fitting procedure), *i.e.*:

$$f(\tilde{\nu}) = M \cdot L(\tilde{\nu}) + (1 - M) \cdot G(\tilde{\nu}) \quad \text{(SI-11)}$$

where *M* denotes the fraction of the Lorentzian $L(\tilde{\nu})$, and (1 – *M*) the fraction of the Gaussian $G(\tilde{\nu})$ contribution, which are given by:

$$L(\tilde{\nu}) = \frac{H}{4 \cdot \left(\frac{\tilde{\nu} - \tilde{\nu}_0}{w}\right)^2 + 1} \quad \text{(SI-12)}$$

$$G(\tilde{\nu}) = H \cdot exp\left[-4\ln 2 \cdot \left(\frac{\tilde{\nu} - \tilde{\nu}_0}{w}\right)^2\right] \quad \text{(SI-13)}$$

In (SI-12) and (SI-13), *H* is the peak height (maximum value) of the function, *w* denotes the full width at half maximum value, while $\tilde{\nu}_0$ is the position of the band center. In the case of $Ni_3(OH)_4(NO_3)_2$, 14 component bands had to be used to generate the reconstructed band shape shown in Fig. 11b in the main text. Note that no deconvolution has been carried out prior to the fitting. The "background" *i.e.* "baseline" in the spectroscopy data has been modelled with linear function in the regions relevant to the figures shown in the manuscript. For a successful fitting of certain other spectral regions, modelling of the background with a second-order polynomial function (a parabola) was required.

Raman spectroscopy results

Aside from the FTIR measurements, we have also carried out Raman spectroscopic investigations of both the intermediates and the final products (NiO-a and NiO-c).

In line with the conclusion drawn from the results obtained by XRD and FTIR spectroscopy, Raman measurements confirm that β-$Ni(OH)_2$ is obtained using ammonia as a hydroxide precursor, Fig. SI-7 a. The Raman spectrum contains all four expected bands according to the prediction of the factor group theory performed on the basis of the symmetry of β-$Ni(OH)_2$, two with E_g and two with A_{1g} symmetry, appearing at 310-315 cm^{-1}, 445-453 cm^{-1}, 880 cm^{-1} and 3581 cm^{-1}, respectively.

Raman spectrum of the $Ni_3(OH)_4(NO_3)_2$ intermediate is presented in Fig. SI-7 b. Along with the Raman-active modes involving lattice OH stretch and bend modes, the spectrum contains additional bands due to NO_3^- and H_2O species. Since positions of some of these bands are close to the positions of bands characteristic for free NO_3^- ions and H_2O molecules, it confirms that the synthesized intermediate phase contains free NO_3^- ions and H_2O molecules intercalated in the interlayer space. These results complement the results and conclusions for turbostratic structure of the $Ni_3(OH)_4(NO_3)_2$ intermediate, as discussed in details in the main text of the manuscript.

Fig. SI-7 c and d show the Raman spectra of the NiO NPs obtained from the two precursors (NiO-a and NiO-c). The most intense band at ~ 509 cm^{-1} along with the shoulder peak at ~ 195 cm^{-1} have been assigned to the first order phonon modes of the NiO NPs, while the weak and wide bands at ~ 869 cm^{-1} and ~ 1056 cm^{-1} are due to the second order phonon modes of the NiO NPs. The issues concerning the nature of the first-order phonon modes as well as the influence of confinement on their properties are discussed in more details in the main text of the manuscript.

It is worth mentioning that, for the purpose of the present study, the data obtained with Raman spectroscopy serve as a complementary set to those obtained from FTIR measurements. For example, the two OH stretching modes are of different symmetries (the symmetric OH stretch is of A_{1g} symmetry type, while the antisymmetric one is of A_{2u} symmetry type). As a consequence of different parity types, the symmetric stretch is Raman active, while the antisymmetric stretch is IR active (Fig. SI-8). This property opens the possibility for a complementary use of the two spectroscopic techniques in this study to follow the fate of the hydroxide species upon thermal treatment of the intermediates obtained by the two different synthetic routes.

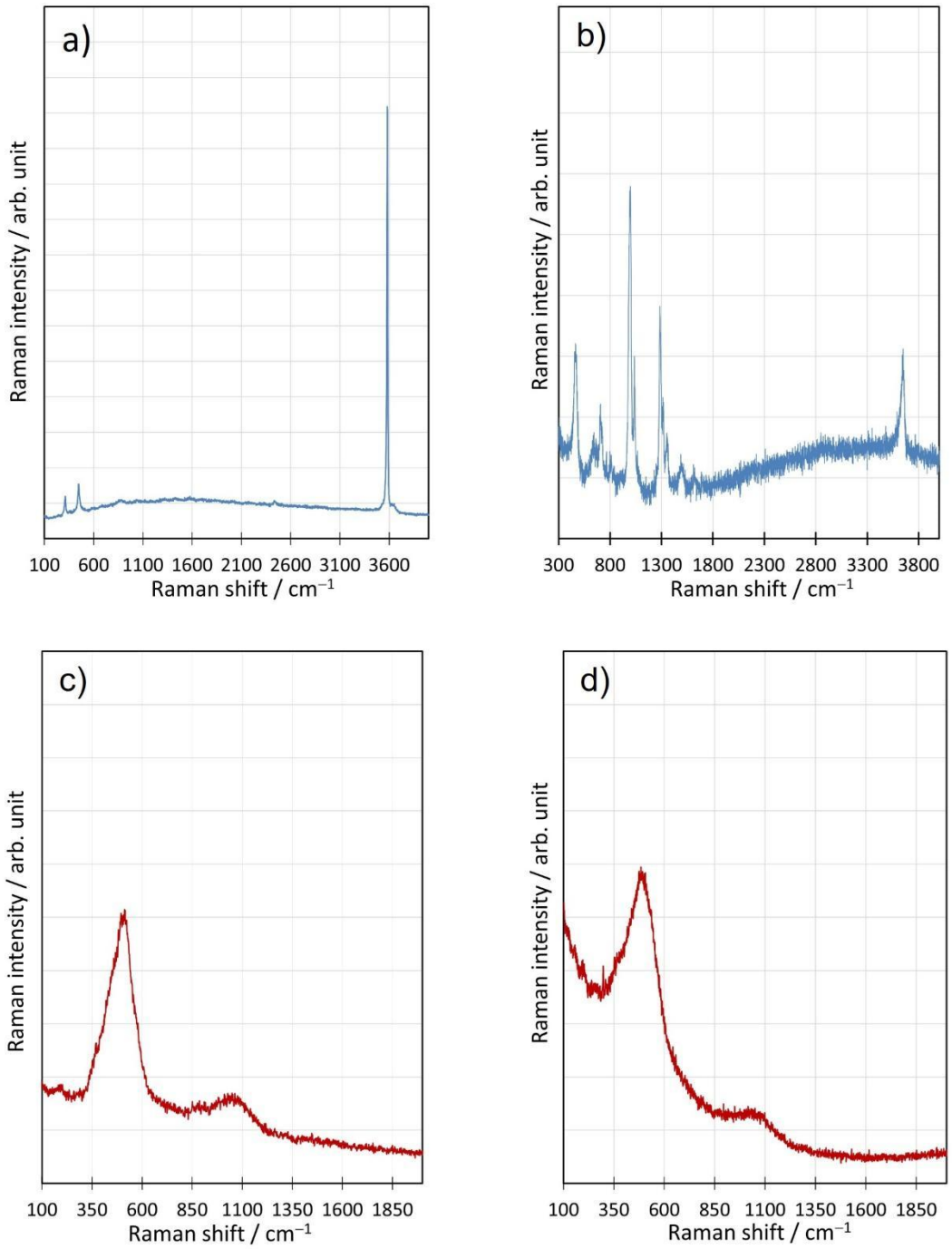

Fig. SI-7. Raman spectra of hydroxide phases synthesized from ammonia (a) and carbamide (b) based reaction system and corresponding NiO phases (c) and (d).

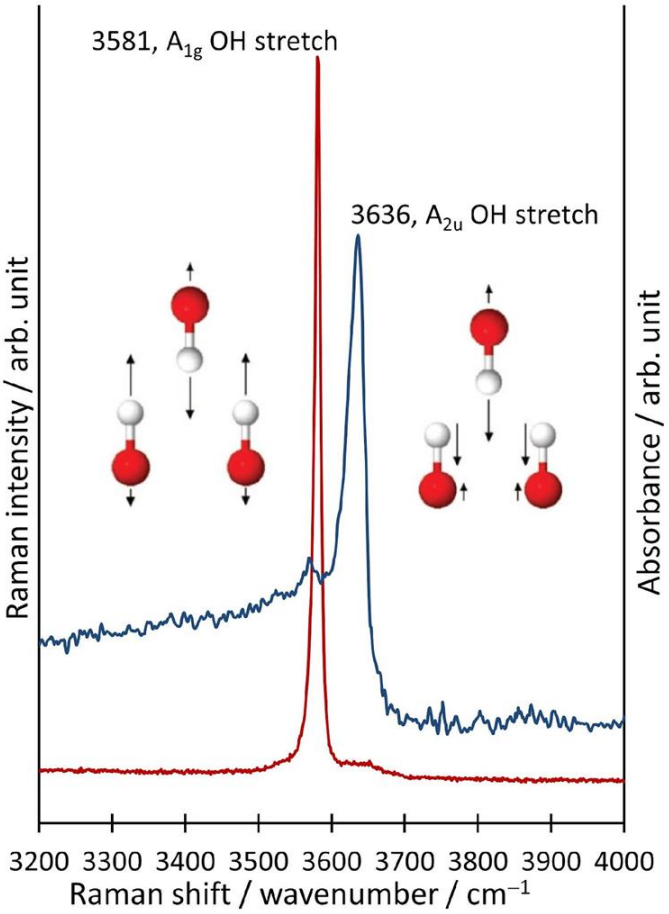

Fig. SI-8. The two OH stretching modes of different symmetries (the symmetric OH stretch of A_{1g} symmetry type, and the antisymmetric one of A_{2u} symmetry type) in the structure of $Ni(OH)_2$. As a consequence of different parity types, the symmetric stretch is Raman active, while the antisymmetric stretch is IR active.

Additional data related to the low dimensionality effects on the phonon modes studied by Raman spectroscopy

Table SI-2. Summary of the most important parameters obtained from reconstruction of the region of the fundamental TO, SO and LO phonon bands in the Raman spectra of the nickel oxide phases obtained from β-$Ni(OH)_2$ (NiO – a) and $Ni_3(OH)_4(NO_3)_2$ (NiO – c) intermediates (band center - $\tilde{\nu}_0$, band integral intensity – *I*, full width at half maximum intensity – *w*, and the calculated phonon lifetime – τ).

Final product	mode	$\tilde{\nu}_0$ / cm^{-1}	*I* / arb. units	*w* / cm^{-1}	τ / fs
NiO – a	TO	369.3	577.8	44.6	119.1
	SO	433.8	3104.7	89.8	59.1
	LO	509.9	13764.9	117.8	45.1
				I(SO)/*I*(TO)	5.373
				I(SO)/*I*(LO)	0.226
NiO – c	TO	385.0	143.3	48.2	110.2
	SO	424.4	21.3	9.9	537.6
	LO	491.4	1455.0	105.6	50.3
				I(SO)/*I*(TO)	0.149
				I(SO)/*I*(LO)	0.015

SI-REFERENCES

[SI-REF-1] Noda, I. Generalized two-dimensional correlation method applicable to infrared, Raman, and other types of spectroscopy. *Appl. Spectrosc.* 1993, 47, 1329-1336.

[SI-REF-2] Noda, I. Determination of two-dimensional correlation spectra using the Hilbert transform. *Appl. Spetrosc.* 2000, 54, 994-999.

[SI-REF-3] Thomas, M.; Richardson, H. H. Two-dimensional FT0IR correlation analysis of the phase transitions in a liquid crystal, 4'-*n*-octyl-4-cyanobiphenyl (8CB). *Vib. Spectrosc.* 2000, 24, 137-146.

[SI-REF-4] Morita, S.; Shinzawa, H.; Tsenkova, R.; Noda, I.; Ozaki, Y. Computational simulations and a practical application of moving-window two-dimensional correlation spectroscopy. *J. Mol. Struct.* 2006, 799, 111-120.

[SI-REF-5] Biesinger, M. C.; Payne, B. P.; Lau, L. W. M.; Gerson, A.; Smart, R. St. C. X-ray photoelectron spectroscopic chemical state quantification of mixed nickel metal, oxide and hydroxide systems. *Surf. Interface Anal.* 2009, 41 324-332.

[SI-REF-6] Biesinger, M. C.; Payne, B. P.; Grosvenor, A. P.; Lau, L. W. M.; Gerson, A.; Smart, R. St. C. Resolving surface chemical states in XPS analysis of first row transition metals, oxides and hydroxides: Cr, Mn, Fe, Co and Ni. *Appl. Surf. Sci.* 2011, 257, 2717-2730.

[SI-REF-7] Grosvenor, A. P.; Biesinger, M. C.; Smart, R. St. C.; McIntyre, N. S. New interpretations of XPS spectra of nickel metal and oxides. *Surf. Sci.* 2006, 600, 1771-1779.

[SI-REF-8] Preda, I.; Mossanek, R. J. O.; Abbate, M.; Alvarez, L.; Mendez, J.; Gutierrez, A.; Soriano, L. Surface contributions to the XPS spectra of nanostructured NiO deposited on HOPG. *Surf. Sci.* 2012, 606, 1426-1430.

[SI-REF-9] Gupta, R. P.; Sen, S. K. Calculation of multiplet structure of core *p*-vacancy levels. II. *Phys. Rev. B* 1975, 12, 11-19.

[SI-REF-10] Mansour, A. N. Characterization of NiO by XPS. *Surf. Sci. Spectra* 1996, 3, 231-238.

[SI-REF-11] Biesinger, M. C.; Lau, L. W. M.; Gerson, A.; Smart, R. St. C. The role of Auger parameter in XPS studies of nickel metal, halides and oxides. *Phys. Chem. Chem. Phys.* 2012, 14, 2434-2442.